Noor A. Hakim
Ameera O.H. Al-Janabi

Department of Environmental Pollution,
College of Environmental Science,
Al-Qasim Green University
Babil Governorate, IRAQ

Influence of Copper Oxide Top Layer on Structural and Optical Properties of Tin Sulfide Thin Films Deposited by Spray Pyrolysis

In this work, the effect of the upper cupric oxide (CuO) layers by spray pyrolysis on the optical and structural characteristics of tin sulfide (SnS) thin films was investigate. The SnS film displays dual phases of orthorhombic and Zincblende and the appearance of a monoclinic CuO phase after the deposition of the upper layer. The field emission scanning electron microscopy (FE-SEM) reveals notable variations in surface characteristics after deposition of the top layer. The general increase in optical absorbance with no alterations in the optical bandgap (2 eV) was demonstrated. The photoluminescence test (PL) shows the characteristic emission peaks at 485nm (2.55eV) attributed to S vacancies and lattice defects and 550nm (2.25eV) band-to-band transitions. Additional PL peaks corresponding to the CuO structure were observed at 395nm (3.14eV) for the double-layered samples. The results indicate that modifying the optical and structural characteristics of CuO/SnS heterostructures makes them suitable for use in numerous applications.

***Keywords*:** Tin sulfide; Copper oxide; Spray pyrolysis; Optical properties
Received: 10 September 2024; **Revised:** 30 October; **Accepted:** 06 November 2024

1. Introduction

Tin sulfide (SnS) is a p-type semiconductor with a zincblende or orthorhombic crystal structure [1]. SnS thin films have been extensively studied due to their remarkable optical, electrical, and structural properties [2]. The multifunctional potential of SnS thin films has been demonstrated in numerous scientific and technological applications [3]. SnS thin films have been applied for thin-film photodetectors [4]. SnS layers are suitable in thin-film solar cells due to their high absorption coefficient to visible light, significant carrier mobility, and favorable band gap [5]. SnS have been used in gas-sensing applications to detect toxic gases [6]. SnS thin films have been used in photocatalytic applications [7].

One approach is to modify the SnS properties by transforming them into nanostructures to increase their surface area and modify optical properties to improve light absorption and electrical properties to increase carrier mobility and reduce recombination rate [8]. These strategies include constructing various forms of SnS nanostructures [9]. Introducing foreign atoms into the SnS matrix by doping is a well-known strategy for property modification. Doping can improve material properties for specific applications [10]. Annealing, plasma, and chemical treatments performed after deposition can modify the properties of the resulting films [11].

Creating heterojunctions by depositing nanoparticles as a top layer of another material can improve charge separation and carrier mobility [12]. This technique benefits applications that rely on surface interactions, such as photocatalysis and gas sensing applications [13]. By depositing top layers of different semiconductors, charge transfer occurs, and an interfacial depletion region is created along the energy band-bending within the interface [14]. The specific application of the film depends on the chosen deposition technique. Spray deposition produces a rough surface, thereby increasing its surface area. Spray pyrolysis techniques can control film thickness, morphology, and crystallinity [15].

This study aimed to investigate the effect of CuO top layer at different thicknesses, applied by spray pyrolysis, on the properties of SnS thin films. The study examined the structural and optical properties of the applied coating. In addition, the study investigated the possible uses of these modified films.

2. Experimental Part

Tin chloride ($SnCl_2.2H_2O$) and sodium thiosulfate ($Na_2S_2O_3.5H_2O$) were procured from Sigma-Aldrich and were used without further purification. $SnCl_2.2H_2O$ and $Na_2S_2O_3.5H_2O$ were dissolved separately in distilled to form 0.1 M for each on magnetic stirrer and then mixed to create the started solution for deposition of the tin sulphide (SnS) thin film by spray pyrolysis at 400 °C substrate temperature. The upper layers of CuO were deposited onto the SnS surface using different volumes of 0.1 M $CuCl_2.2H_2O$ solution. The samples resulting in CuO/SnS heterostructure were labelled SC1, SC2, SC3, and SC4, corresponding to the different sprayed volumes of $CuCl_2.2H_2O$ solution (0.5, 1, 1.5, and 2 ml), respectively. The structural, surface morphology and optical properties of the as-deposited layers were characterized using X-ray diffraction (XRD) with a Shimadzu XRD 6000 instrument, scanning electron microscopy (SEM) with a JSM-

7600F JEOL microscope, Fourier transform infrared spectroscopy (FTIR) from Shimadzu, ultraviolet-visible absorption spectroscopy with an SP-8001 spectrophotometer, and photoluminescence spectroscopy.

3. Results and Discussions

Figure (1) shows the XRD patterns of SnS and CuO/SnS thin films prepared by spray pyrolysis. Different upper-layer thicknesses of CuO, achieved by varying the spray volume of copper chloride, were deposited onto the SnS thin films labelled CS1, CS2, CS3, and CS4, respectively. The XRD patterns of the SnS thin film illustrate numerous diffraction peaks corresponding to the SnS orthorhombic and metastable phase of Zincblende according to standard data of JCPDF numbers 01-071-3678 and 00-039-0354, respectively. The films prepared using the simple spray pyrolysis technique can be used in various applications based on their crystalline structures [16].

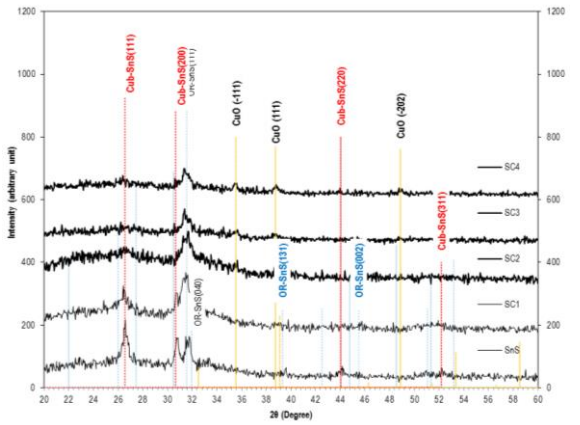

Fig. (1) XRD patterns of the SnS and double-layered CuO/SnS thin films

Deposition of the upper layer of CuO appeared as an additional phase with diffraction peaks positioned at 2θ= 35.6°, 38.7°, and 48.8°, corresponding to the monoclinic CuO crystalline planes (-111), (111), and (-202), respectively, according to the JCPDF database No 96-101-1195. The intensity of the CuO diffraction peaks increased with increasing the spray volume on the upper layer, indicating enhanced crystallinity, attributed to the availability of additional materials for grain growth, leading to larger grains with a more ordered crystal structure. The Bragg equation was used to determine the inter-planar atomic spacing (d_{hkl}) [17], whereas Scherrer's formula was utilized to calculate the crystallite size values (D) [18], as detailed in table (1). Both cubic and orthorhombic phases showed a reduction in crystallite size with increasing the upper CuO layer thickness.

Figure (2) shows the calculated phases' ratios according to the XRD peaks' intensities, corresponding to each phase, for the SnS and CuO/SnS thin-film samples at different upper-layer thicknesses. The figure shows a higher presence of zincblende SnS phases than orthorhombic ones and is nearly equal with increasing the upper layer by reducing the existence of zincblende phase while increasing the CuO phase. Orthorhombic phase is the most thermodynamically stable phase of SnS. Orthorhombic phase is more suitable than zinc blend phase for photo absorption applications, making it suitable for solar cell and optoelectronic applications [19].

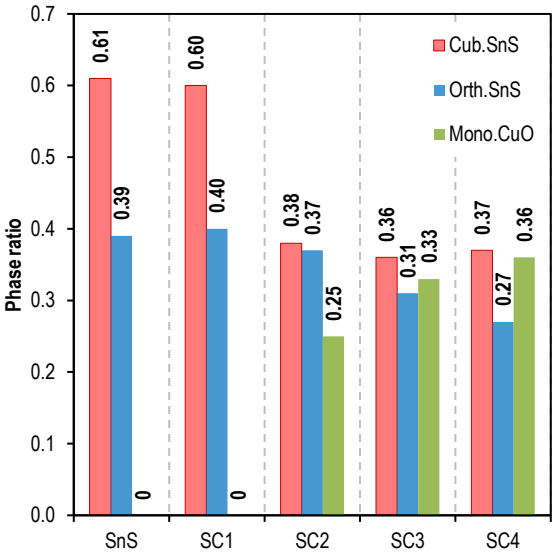

Fig. (2) Cubic, orthorhombic-SnS, and monoclinic-CuO ratios according to diffraction line intensity

Figure (3) shows the FE-SEM images of the CuO/SnS surface at different upper-layer thicknesses. The FE-SEM results provide insights into surface morphology variations with increasing the upper-layer thickness, which is crucial for evaluating their potential in photocatalytic and gas-sensing applications. Sample SC1 exhibited low porosity initially, but flake-like structures were formed irregularly oriented across the surface. Increasing the thickness of the upper layer caused significant variations in surface morphology, with the development of a porous structure in SC2 and cauliflower-like nanostructures in SC3. Finally, these nanostructures became more porous in sample SC4, forming highly ramified structures with high porosity and surface area. These observations emphasize the usefulness of CuO/SnS thin films in enhancing the sample surface for use in various fields.

The Fourier-transform infrared (FTIR) spectra of the bare SnS and CuO-coated thin films at various sprayer solution volumes in the upper layer are shown in Fig. (4). The test was conducted between 400 and 4000 cm^{-1}. The FTIR spectrum of SnS shows the characteristic absorption bands. The bands at 837.86 and 785.42 cm^{-1} correspond to Sn-S vibrations [20,21], which point to the formation of the tin sulfide structure. Additional bands attributable to adsorbed water

molecules and carbonyl groups from the ambient environment were found at 3404.80 cm^{-1} for -OH stretching, 2917.10 and 2846.30 cm^{-1} for CH2 stretching, and 1650.70 cm^{-1} for O-H bending [22]. Additionally, bands at 1286.21, 1215.45, and 1155.15 cm^{-1} match the S-O band [23], indicating the possibility of some sulfur oxide phases.

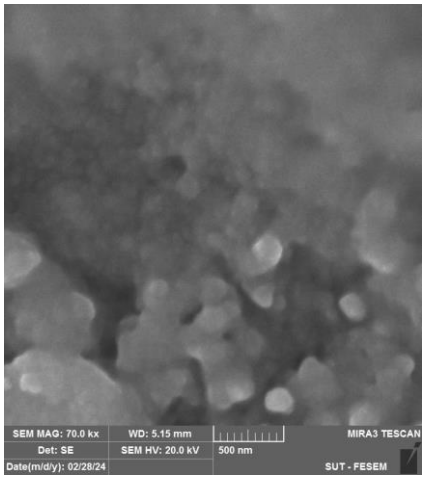

(SC1)

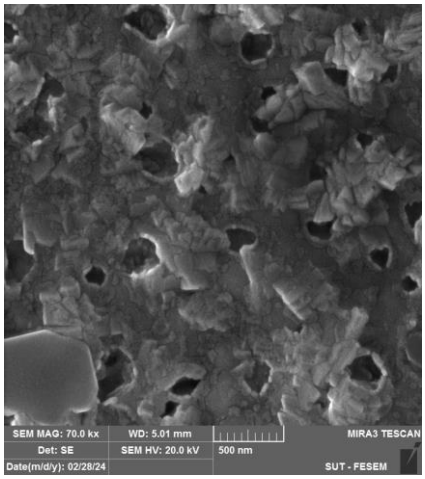

(SC2)

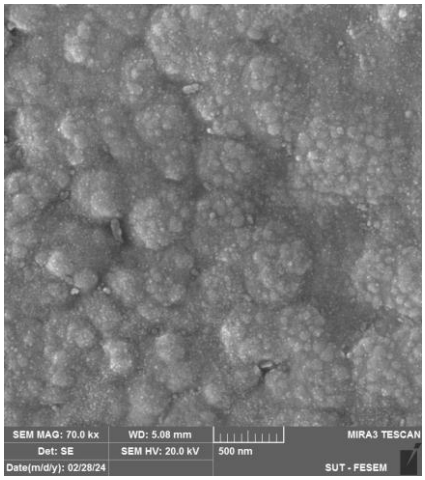

(SC3)

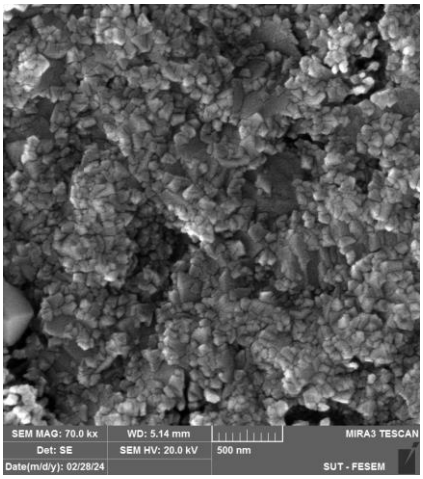

(SC4)

Fig. (3) FE-SEM images of the double-layered CuO/SnS thin films at different upper-layer thicknesses

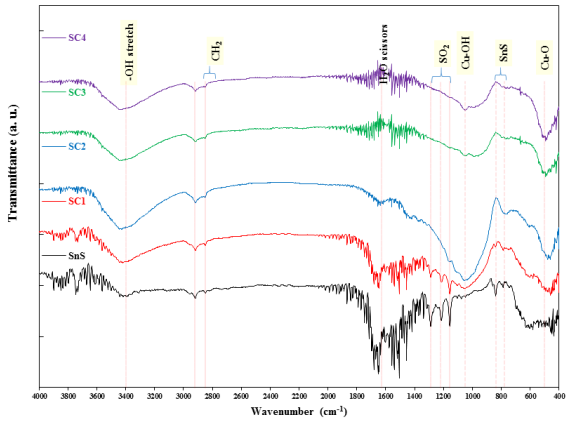

Fig. (4) FTIR transmission curves of the SnS thin film and the film-coated by an upper layer of CuO with different amounts of its precursor solution

Some variations were observed after depositing the upper CuO layer. The CuO layer introduces additional broad bands at 1053.18 and 462.81 cm^{-1}, corresponding to Cu-OH and Cu-O vibrations, respectively [24], which indicates the presence of metastable metal hydroxide in addition to the copper oxide phase. Other variations in the patterns include reductions in the intensities of some peaks and slight shifts. These changes can be attributed to the alteration of the band energies of certain bands due to interactions with the upper layer during the deposition process. Table (2) lists the bands for the SnS sample and those coated with CuO at different thicknesses.

Figure (5) illustrates the absorption spectra and energy bandgap of bare SnS thin films and those coated with CuO at varying thicknesses (samples SC1, SC2, SC3, and SC4) within the wavelength range 300–1100 nm. The spectra exhibit a decline in absorption with wavelength, with a gradual absorption edge around 600 nm. The non-sharp absorption edge is due to the low

degree of crystallinity, that is, due to the presence of crystalline defects that form local levels near the conduction band. Increasing the CuO thickness increased the optical absorbance. The improved absorbance indicates that the sample capability for harvesting solar energy can be enhanced in photonic applications such as solar cells [25,26], selective absorbers [27], and photocatalysis [28].

Table (2) FTIR bands of SnS and CuO/SnS thin films at different upper-layer thicknesses

Band Type	SnS	SC1	SC2	SC3	SC4
O-H stretch	3404.80	3412.14	3432.24	3429.73	3432.24
CH_2	2917.10	2917.24	2914.72	2917.24	2917.24
	2846.30	2849.41	2849.41	2849.41	2849.41
H_2O	1650.70	-	1636.01	-	-
SO_2	1286.21	1286.81	-	-	-
	1215.45	1216.47	-	-	-
	1155.15	1153.66	-	-	-
Cu-OH	-	-	1053.18	1050.66	1045.64
SnS	837.86	837.13	-	-	-
	785.42	786.88	776.83	-	-
Cu-O	-	460.29	462.81	487.93	487.93

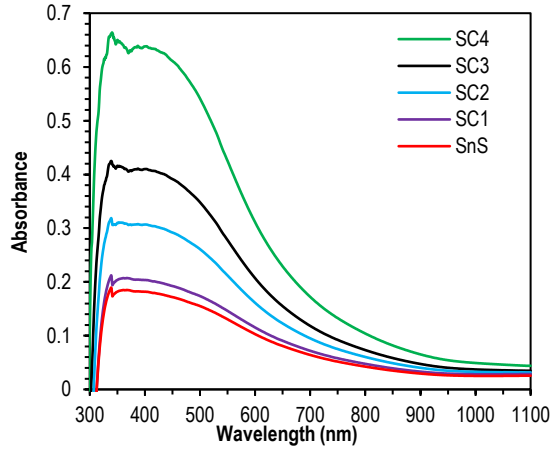

(a)

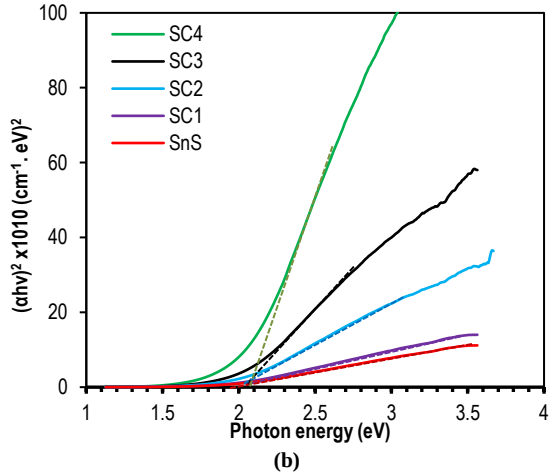

(b)

Fig. (5) UV-visible absorbance spectra (a) and Tauc plot (b) of SnS and CuO/SnS thin films (samples SC1, SC2, SC3, and SC4)

The optical energy bandgap (E_g^{opt}) was determined using the Tauc relation, as illustrated in Fig. (5b). The optical energy gap varied nearly constant at approximately 2 eV following the deposition of the upper CuO layer at different thicknesses.

Figure (6) displays the photoluminescence spectra of SnS and CuO/SnS thin films at different upper-layer thicknesses (samples SC1, SC2, SC3, and SC4) in the wavelength range 350–600 nm using an excitation source at a wavelength of 300 nm.

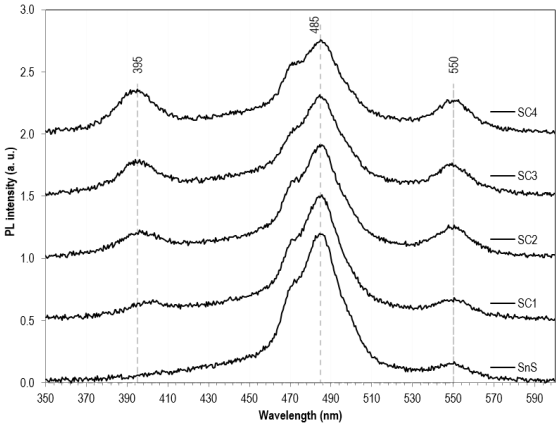

Fig. (6) PL spectra of the SnS and CuO/SnS thin films

Two broad peaks can be observed in the SnS sample. The emission around 485 nm wavelength (2.55 eV) is attributed to S vacancies and lattice imperfections in the SnS crystal [29]. In contrast, the emission at a wavelength of around 550 nm (2.25 eV) is associated to band-to-band transitions [30,31]. An additional emission peak appeared at 395 nm (3.14 eV) after deposition of the upper layer, corresponding to the band-to-band transition of CuO. This emission line increased in intensity as the upper layer thickness increased. The additional peak indicates the formation of Copper oxide nanoparticles on the sample surface. Almost no variations were observed in the positions of the SnS bands after the deposition of the upper CuO layer.

4. Conclusions

In this work, a new, simple and inexpensive strategy was adopted to modify the properties of SnS thin films and its adaptability for use in various applications was evaluated. Spray pyrolysis-based top-layer CuO deposition on SnS thin films was proven to modify the structural and optical characteristics of SnS by forming CuO/SnS heterostructures. The structural investigation confirmed the crystalline character of SnS films with mixed phases of zinc bleached and orthorhombic structures and an additional monoclinic CuO phase formed after the deposition of the upper layer and modifying the phase ratio. The deposition of the upper CuO layer has modification with high porosity. CuO nanoparticles are indicated by the emergence of an extra CuO emission peak and different emissions, which correspond to S vacancies and band-to-band

transitions. The top layer increased the sample absorbance, whereas the optical bandgap unchanged. There are various advantages to the CuO upper layer. First, the addition of more lattice defects can increase surface reactivity. Additionally, the formed CuO/SnS heterojunctions enhance the charge separation and improve the optoelectronic performance. The specific characteristics of the CuO/SnS heterojunction enhance the light absorption and charge-carrier transport in photocatalysis, making it a possible application.

References

[1] C. Gao, H. Shen and L. Sun, "Preparation and properties of zinc blende and orthorhombic SnS films by chemical bath deposition", *Appl. Surf. Sci.*, 257 (2011) 6750–6755.

[2] K.J. Norton, F. Alam and D.J. Lewis, "A review of the synthesis, properties, and applications of bulk and two-dimensional tin (II) sulfide (SnS)", *Appl. Sci.*, 11 (2021) 1–36.

[3] N. Aparna, R.S. Philip and M. Mathew, "Photocatalytic activities of SnS thin films deposited at room temperature", *Appl. Surf. Sci. Adv.*, 13 (2023) 100374.

[4] M.S. Mahdi et al., "A highly sensitive flexible SnS thin film photodetector in the ultraviolet to near infrared prepared by chemical bath deposition", *RSC Adv.*, 6 (2016) 114980–114988.

[5] S.-I. Son et al., "Effect of working pressure on the properties of RF sputtered SnS thin films and photovoltaic performance of SnS-based solar cells", *J. Alloys Comp.*, 831 (2020) 154626.

[6] Y.G. Song et al., "Cross-linked structure of self-aligned p-type SnS nanoplates for highly sensitive NO_2 detection at room temperature", *J. Mater. Chem. A.*, 10 (2022) 4711–4719.

[7] A. Taufik, R. Saleh and G. Seong, "Enhanced photocatalytic performance of SnS_2 under visible light irradiation: strategies and future perspectives", *Nanoscale*, 4 (2024) 1–15.

[8] D. Mudusu et al., "Growth of single-crystalline cubic structured tin(II) sulfide (SnS) nanowires by chemical vapor deposition", *RSC Adv.*, 7 (2017) 41452–41459.

[9] A. Javed et al., "Thickness dependent structural, electrical and optical properties of cubic SnS thin films", *Mater. Chem. Phys.*, 246 (2020) 122831.

[10] V.P. Jethwa et al., "Enhanced electrical and optoelectronic performance of SnS crystal by Se doping", *J. Alloys Comp.*, 883 (2021) 160941.

[11] F. Alam and V. Dutta, "Tin sulfide (SnS) nanostructured films deposited by continuous spray pyrolysis (CoSP) technique for dye-sensitized solar cells applications", *Appl. Surf. Sci.*, 358 (2015) 491–497.

[12] F. Djeffal et al., "Performance analysis of SnS photodetector using strained SnO_2 stacked layer: Numerical simulation and DFT calculations", *Microelectron. Eng.*, 273 (2023) 111961.

[13] Y. Liu et al., "Electrodeposition of copper-doped SnS thin films and their electric transmission properties control for thermoelectric enhancement", *J. Mater. Sci. Mater. Electron.*, 30 (2019) 15880–15888.

[14] S. Das et al., "Decoration of laser-ablated ZnO nanoparticles over sputtered deposited SnO_2 thin film based formaldehyde sensor", *Sens. Actuat. B Chem.*, 367 (2022) 132114.

[15] M.O. Salman, M.A. Kadhim and A.A. Khalefa, "CdO:SnO_2 Composite UV-Assisted Room Temperature Ozone Sensor", *Iraqi J. Sci.*, 64 (2023) 1190–1202.

[16] L.A. Burton and A. Walsh, "Phase Stability of the Earth-Abundant Tin Sulfides SnS, SnS_2, and Sn_2S_3", *J. Phys. Chem. C*, 116 (2012) 24262−24267.

[17] R.O. Gould and W. Massa, **"Crystal Structure Determination"**, Springer (Berlin Heidelberg, 2013).

[18] J.R.H. Ross, "Catalyst Characterization", Ch. 5, in: J.R.H. Ross (Ed.), **"Contemporary Catalysis"**, Elsevier (Amsterdam, 2019), pp. 121–132.

[19] P.C. Huang et al., "Photoelectrochemical properties of orthorhombic and metastable phase SnS nanocrystals synthesized by a facile colloidal method", *Thin Solid Films*, 596 (2015) 135–139.

[20] J. Srivind et al., "Visible light irradiated photocatalytic and magnetic properties of Fe-doped SnS_2 nanopowders", *J. Mater. Sci. Mater. Electron.*, 29 (2018) 9016–9024.

[21] M.A. Dar, D. Govindarajan and G.N. Dar, "Facile synthesis of SnS nanostructures with different morphologies for supercapacitor and dye-sensitized solar cell applications", *J. Mater. Sci. Mater. Electron.*, 32 (2021) 20394–20409.

[22] H. Hajifatheali et al., "The synthesis of N-methylbis[2-(dodecylthio)ethyl]amine (SNS) and investigation of its efficiency as new mononuclear catalyst complex in copper-based ATRP", *Macromol. Res.*, 23 (2015) 977–985.

[23] O.G. Buzykin et al., "Spectroscopic detection of sulfur oxides in the aircraft wake", *J. Russ. Laser Res.*, 26 (2005) 402–426.

[24] M. Shafiey Dehaj and M. Zamani Mohiabadi, "Experimental study of water-based CuO nanofluid flow in heat pipe solar collector", *J. Therm. Anal. Calorim.*, 137 (2019) 2061–2072.

[25] N. Jahan et al., "A comparative study of CuO based solar cell with ZnTe HTL and SnS2 ETL using SCAPS 1D simulation", *J. Opt.*, (2024). https://doi.org/10.1007/s12596-024-01800-6.

[26] M.A. Hameed, S.H. Faisal and R.H. Turki, "Characterization of Multilayer Highly-Pure Metal Oxide Structures Prepared by DC Reactive Magnetron Sputtering Technique", *Iraqi J. Appl.*

Phys., 16(4) (2020) 25-30
[27] G.G. Welegergs et al., "Single-Layered Biosynthesized Copper Oxide (CuO) Nanocoatings as Solar-Selective Absorber", *Appl. Sci.*, 13 (2023) 1–15.
[28] M. Arafa, Y. Abdelmonem and M. Madkour, "Visible active narrow/narrow band gap CuO/Cu_2SnS_3 nanoheterostructures as efficient nanophotocatalysts", *J. Chem. Phys.*, 158 (2023). https://doi.org/10.1063/5.0135211.
[29] S. Sebastian et al., "Enhancement in photovoltaic properties of Nd:SnS films prepared by low-cost NSP method", *Rare Met.*, 41 (2022) 1661–1670.
[30] D. Vikraman et al., "Shape- and size-tunable synthesis of tin sulfide thin films for energy applications by electrodeposition", *Appl. Surf. Sci.*, 479 (2019) 167–176.
[31] A.M. Hameed and M.A. Hameed, "Spectroscopic characteristics of highly pure metal oxide nanostructures prepared by DC reactive magnetron sputtering technique", *Emergent Materials*, 6 (2022) 627-633.

Table (1) XRD diffraction angles, d_{hkl} values, corresponding Miler indices, and phases of the bare SnS and double-layered CuO/SnS thin films

Sample	2θ (Deg.)	FWHM (Deg.)	d_{hkl} Exp.(Å)	D (nm)	Phase	hkl
SnS	26.6172	0.5090	3.3463	16.0	Cubic SnS	(111)
	27.2959	0.3182	3.2646	25.7	Orth. SnS	(021)
	30.7953	0.3605	2.9011	22.9	Cubic SnS	(200)
	31.5376	0.2757	2.8345	29.9	Orth. SnS	(111)
	31.7497	0.3817	2.8161	21.6	Orth. SnS	(040)
	39.5758	0.3606	2.2754	23.4	Orth. SnS	(131)
	44.1782	0.4454	2.0484	19.2	Cubic SnS	(220)
	45.5143	0.2758	1.9913	31.2	Orth. SnS	(002)
	52.2163	0.2757	1.7504	32.1	Cubic SnS	(311)
SC1	26.4848	0.6421	3.3627	12.7	Cubic SnS	(111)
	30.7651	0.3210	2.9039	25.7	Cubic SnS	(200)
	31.5142	0.7100	2.8366	11.6	Orth. SnS	(111)
	45.6394	0.4708	1.9862	18.3	Orth. SnS	(002)
SC2	26.5918	0.7063	3.3494	11.6	Cubic SnS	(111)
	31.5784	0.7500	2.8310	11.0	Orth. SnS	(111)
	35.5163	0.3852	2.5256	21.7	Mono. CuO	(-111)
	38.6624	0.4066	2.3270	20.7	Mono. CuO	(111)
SC3	31.4714	0.7700	2.8403	10.7	Orth. SnS	(111)
	35.5805	0.4280	2.5212	19.5	Mono. CuO	(-111)
	38.7052	0.4922	2.3245	17.1	Mono. CuO	(111)
	48.8283	0.7277	1.8636	12.0	Mono. CuO	(-202)
SC4	31.4072	0.8100	2.8460	10.2	Orth. SnS	(111)
	35.4949	0.3852	2.5270	21.7	Mono. CuO	(-111)
	38.7908	0.4066	2.3196	20.7	Mono. CuO	(111)
	44.0342	0.2997	2.0548	28.6	Cubic SnS	(220)
	48.8497	0.4281	1.8629	20.4	Mono. CuO	(-202)

